THE JOURNAL OF PHYSICAL CHEMISTRY C
A JOURNAL OF THE AMERICAN CHEMICAL SOCIETY

pubs.acs.org/JPCC

Article

Near-Infrared Emission from CdSe-Based Nanoplatelets Induced by Ytterbium Doping

Merve İzmir, Emek G. Durmusoglu, Manoj Sharma, Farzan Shabani, Furkan Isik, Savas Delikanli, Vijay Kumar Sharma, and Hilmi Volkan Demir*

Cite This: J. Phys. Chem. C 2023, 127, 4210−4217

Read Online

ACCESS | Metrics & More | Article Recommendations | Supporting Information

ABSTRACT: Cadmium selenide (CdSe) nanoplatelets (NPLs) have attracted significant attention thanks to their favorable optical properties, including narrow emission linewidths, reduced Auger recombination, and a high absorption cross section. However, the photoluminescence (PL) quantum yield (QY) in the near-infrared (NIR) region is poor as compared to that in the visible region. Doping of metal ions is proven to be a successful strategy for inducing Stokes-shifted NIR emission. Here, we report the first account of the successful doping of ytterbium (Yb) into CdSe NPLs by a modified seeded-growth method. The successful incorporation of divalent Yb ions into CdSe NPLs resulted in an additional NIR emission apart from their excitonic emission. By optimizing the dopant concentration, we observed an impressive PL QY of ∼55% for these Yb-doped NPLs. Detailed elemental and optical characterizations were conducted to understand the emerging photophysical properties of these Yb-doped NPLs. These NIR-emitting lanthanide-doped CdSe NPLs might have applications in the next-generation bioimaging, night vision, and photodetection.

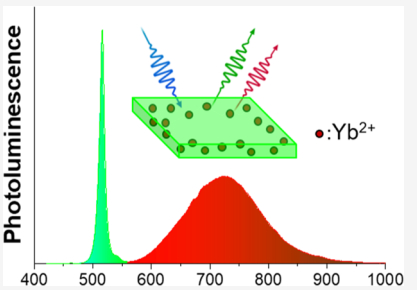

INTRODUCTION

Cadmium selenide (CdSe) nanoplatelets (NPLs) have recently attracted great interest because of their distinguished properties originating from their strong quantum confinement along the *z*-direction. They possess a narrow emission linewidth, giant oscillator strength, a large absorption cross section, and reduced Auger recombination.[1,2] Thanks to these outstanding features, CdSe NPLs can be utilized as an active medium for a vast range of applications that include light-emitting diodes, colloidal quantum well lasers, luminescent solar concentrators, detectors, and phototransistors.[3−8] Typically, CdSe NPLs exhibit emission peaks around 460 nm for three monolayers (MLs), 515 nm for four MLs, and 550 nm for five MLs of thickness, respectively. Therefore, the emission of CdSe NPLs can be tuned by varying the number of MLs (thickness).[9] Moreover, extending the spectral coverage and fine-tuning the photoluminescence (PL) spectra is achieved by shell growth, alloying, and doping techniques.[10−14] In particular, the doping process introduces mid-gap states within the bandgap of the host structure, which leads to a Stokes-shifted emission characterized by a relatively long lifetime.[15−17]

Two of the most studied dopants (Cu and Ag) in II−VI nanocrystals have shown an efficient Stokes-shifted emission with decreased self-absorption.[13,17−21] These dopant ions have a d-orbital state near the valence band, which captures the photoexcited holes.[13] This results in a Stokes-shifted dopant-induced emission for Cu- and Ag-doped semiconductor nanocrystals.[4,18,22] However, doping of lanthanide ions in II−VI nanocrystals is rarely reported. More recently, doping of lanthanide ions (Ln^{3+}) into perovskite nanocrystals has been shown with efficient near-infrared (NIR) luminescence induced by the "2 $F^{5/2}$−2 $F^{7/2}$" transition.[23] Various lanthanide ions have been widely studied as dopants in inorganic crystal lattices.[24] Ideally, Ln^{3+} ions prefer sites with coordination number ≥6.[25] However, there are few reports where CdSe quantum dots (QDs) are doped with Yb^{3+} ions despite possessing a tetrahedral coordination.[26] These Yb^{3+}-doped CdSe QDs were synthesized through a complex three-step synthesis process which yields a poor NIR dopant emission (DE) having PL quantum yield (QY) of less than 1%.[25] On the other hand, divalent Yb exhibits broadband 5d−4f luminescence from an excited $4f^{13}5d^1$ configuration.[26] To the best of our knowledge, Yb-doping for CdSe NPLs has not been reported because of its challenging nature, as Cd ions have a coordination number of 4 and lanthanide ions prefer ≥6 coordination sites. The doping of CdSe NPLs with Yb^{2+} ions is a promising approach to obtain new optical, electrical, and magnetic properties in the field of nanomaterials.[27,28]

Here, we report the synthesis of divalent Yb-doped 4 ML CdSe core NPLs by a modified seeded-growth method. The synthesized CdSe NPLs exhibit dual emission, which comprises

Received: December 29, 2022
Revised: February 1, 2023
Published: February 15, 2023

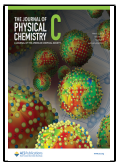

an excitonic emission of ~515 nm and a broad dopant-induced emission in the NIR region emission of ~725 nm. Doping of Yb ions improved the overall PL QY of NPLs from 29 to 55% in the case of 4 ML CdSe core NPLs. Varied Yb-doping in host CdSe NPLs was examined by detailed optical and morphological characterizations. The emission mechanism for these newly added NIR-emitting Yb-doped NPLs is presented and supported with detailed steady-state and transient optical spectroscopies.

METHODS

Chemicals. Cadmium nitrate tetrahydrate, sodium myristate, technical grade 1-octadecene (ODE), selenium, cadmium acetate dihydrate, cadmium iodide, ytterbium iodide, ytterbium acetate, silver acetate, trioctylphosphine (TOP), and technical grade oleic acid (OA) were purchased from Sigma-Aldrich. Methanol, ethanol, acetone, and hexane were purchased from Merck Millipore. Cadmium myristate was synthesized by following a previously reported protocol.[29]

Preparation of Yb-Doping Precursors. For the cationic precursor solution, 0.16 mmol ytterbium iodide (YbI_2) (70.2 mg) and cadmium acetate dihydrate (430 mg) were dissolved in 3.7 mL of ODE and 2.3 mL of OA. The cationic precursor solution was heated at 100 °C until it became transparent. Subsequently, the solution was cooled down to room temperature. Selenium dioxide (27.0 mg) was dissolved in 3 mL of ODE as the anionic precursor, and the solution was heated at 200 °C until a transparent yellow solution was obtained. Cationic and anionic solutions were mixed just before the injection for the seeded growth of the Yb-doped NPLs. YbI_2 concentrations in the cationic precursor were varied to study the effect of varied Yb-dopant amounts in CdSe NPLs. Yb-CdSe NPL-1 (0.16 mmol), Yb-CdSe NPL-2 (0.8 mmol), and Yb-CdSe NPL-3 (0.32 mmol) are labeled according to the amounts of Yb-precursors used in the synthesis.

Synthesis of Yb-Doped CdSe NPLs. To obtain Yb-doped CdSe NPLs, we employed a one-pot, two-step synthesis process by modifying the seeded-growth method.[30] As the first step, we synthesized CdSe NPLs according to our standard recipe. First, 170 mg of cadmium myristate, 12 mg of Se, and 15 mL of ODE were loaded into a 100 mL flask. The solution was degassed and stirred for 1 h at 95 °C. Then, the temperature was set to 240 °C under Ar gas. Cadmium acetate dihydrate was injected swiftly into the reaction at 195 °C, and the reaction was continued at 240 °C for 10 min to provide the growth of 4 ML CdSe NPLs. Then, the seeded-growth method was used to dope Yb as the second step of the synthesis. To achieve that, the Yb precursor solution was added slowly to the as-synthesized CdSe NPLs by using a syringe pump at the rate of 4.5 mL/h for 10 min. The reaction was terminated using 1 mL of OA injection, and the solution was cooled down to room temperature. The NPLs solution was centrifuged at 6000 rpm for 5 min, and the precipitates were dissolved in hexane.

Optical Characterizations. UV−vis absorption and PL spectra of NPLs were obtained using a Shimadzu UV-1800 spectrophotometer and a Shimadzu RF-5301 PC spectrofluorophotometer. For QY measurements, samples were excited with a 405 nm laser (Cobalt Laser) in an integrating sphere, and the data were collected with an Ocean Optics S4000 spectrometer. Time-correlated single-photon counting system with the time resolution down to 4 ps (PicoHarp 300), capable of delivering laser pulses with an 80 MHz repetition rate, was used. It consisted of a picosecond pulsed laser with an output photon energy of 3.31 eV (375 nm) driven by a module (PDL-800 series) and a fast photomultiplier tube (Hamamatsu H5783 series) to resolve the lifetimes on the order of a few picoseconds. Transient absorption (TA) spectroscopy was performed to study the carrier dynamics of the samples by using a Helios setup (Ultrafast Systems LLC) and in the transmission mode with chirp correction. A white light continuum probe beam (400−800 nm) was generated from a 3 mm sapphire crystal using an 800 nm pulse from the regenerative amplifier, as mentioned in the lifetime measurement. The pump beam spot size was ~150 μm. The probe beam passing through the sample was collected using an ultraviolet−visible region detector (CMOS sensor). All measurements were performed at room temperature in hexane.

Structural and Elemental Characterizations. To study the dimension of Yb-doped NPLs, transmission electron microscopy (TEM) images were taken by a JEOL TEM 2100F operated at 200 kV in the high-angle annular dark-field scanning transmission electron microscopy (HAADF−STEM) configuration embedded with an energy-dispersive X-ray spectroscopy (EDX) detector. X-ray photoelectron spectroscopy (XPS) measurements were performed using a Shimadzu Kratos AXIS Nova photoelectron spectrometer to analyze the elemental compositions of Yb-doped CdSe NPLs. The samples were drop-casted on silicon substrates. Their spectra were analyzed by using the Kratos software. All peaks in the XPS scans are referenced to the C 1s peak.

RESULTS AND DISCUSSION

The main challenge of our work was the incorporation of Yb ions into the zinc-blende CdSe NPLs. To date, it has been shown that both Yb^{2+} and Yb^{3+} ions were successfully incorporated into perovskites.[31−33] As in ABX_3 (A = Cs; B = Ca and Sr; X = Cl, Br, and I) perovskites, the B site cations have the coordination number of 6, which is suitable for the doping of $Ln^{2+/3+}$ ions. On the other hand, for the zinc blende CdSe NPLs, the Cd^{2+} ions occupy tetrahedral sites with a coordination number of 4, which perturbs the successful doping of Yb^{3+} ions into the CdSe NPLs.

As reported earlier, efficient doping of Yb^{3+} ions in II−VI nanocrystals is challenging; hence, we used YbI_2 as a source instead for performing doping in the CdSe NPLs. Since YbI_2 possesses a divalent ionic nature, it may be suitable for doping in zinc-blende CdSe NPLs possessing tetrahedral coordination at the Cd ions. Here, we have adopted a modified seeded-growth method as previously reported for Hg doping in CdSe NPLs.[30] This one-pot reaction consists of a two-step reaction: the synthesis of the as-synthesized 4 ML CdSe NPLs and the doping of Yb ions. First, 4 ML CdSe NPLs were synthesized according to our previously reported method.[34,35] Then, a Yb^{2+} precursor solution containing Cd^{2+} cation and Se^{2-} anion precursors was injected using a syringe pump (Figure 1). This method has two essential advantages over in situ synthesis: (1) the morphology (shape, thickness, and lateral size) of host CdSe NPLs is not affected by the doping and their change in concentrations and (2) the incorporation of Yb^{2+} dopants would be more accessible

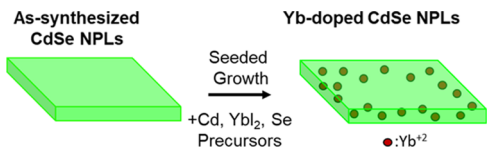

Figure 1. Schematic representation of the synthesis of Yb-doped CdSe NPLs.

https://doi.org/10.1021/acs.jpcc.2c09075
J. Phys. Chem. C 2023, 127, 4210−4217

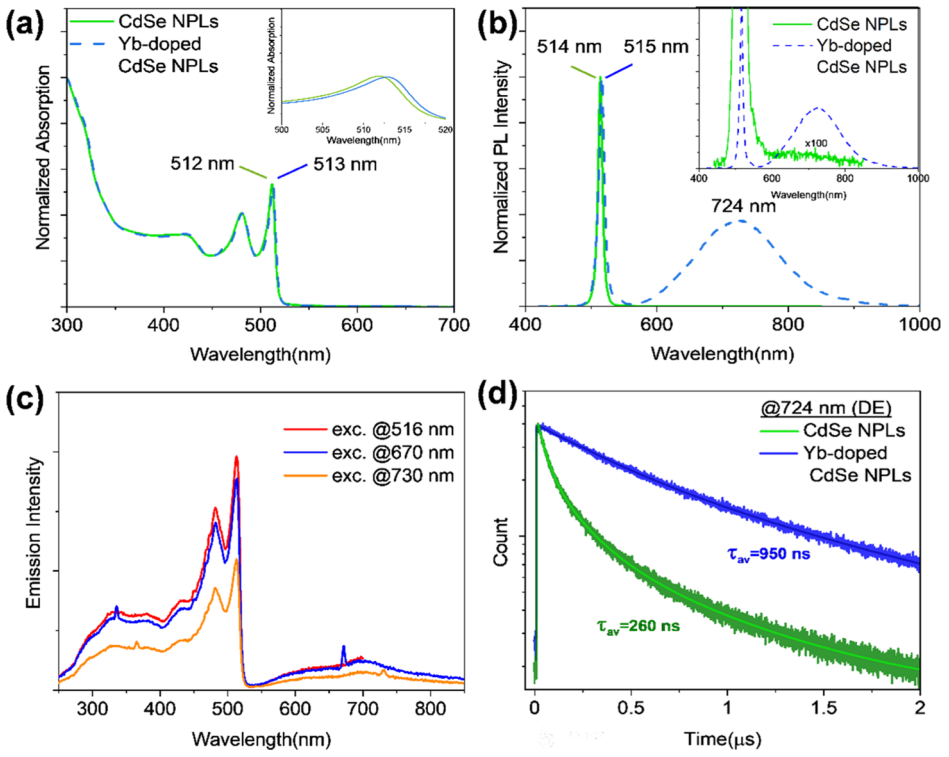

Figure 2. (a) Normalized absorption and (b) PL spectra of undoped and Yb-doped 4 ML CdSe core NPLs. In the inset spectra, the emission intensity of undoped NPLs is multiplied 100 times. (c) PLE spectra of Yb-doped 4 ML CdSe core NPLs. (d) TRF decay curves for the Yb-doped 4 ML CdSe NPLs at the DE.

through exposed Cd^{2+} sites, located at the side surfaces of the core CdSe NPLs. Considering these advantages, we used this modified method in the rest of our study to optimize Yb-doping into CdSe NPLs. Details of the synthesis are presented in the Methods section, and additional experiments with different Yb ions are presented in the Supporting Information (Figures S1 and S2).

Figure 2a–c depicts steady-state absorption, steady-state PL, and photoluminescence excitation (PLE) spectroscopies of undoped and Yb-doped 4ML CdSe NPLs. Absorption spectra of the samples demonstrate that both electron heavy-hole (hh) and electron light-hole (lh) transitions of 4 ML CdSe NPLs remain the same after doping. Martín-Rodríguez et al. reported that Ln^{3+} ions possess weak and narrowband absorption lines, which is in agreement with our findings.[25] The PL emission spectrum of the undoped CdSe NPLs demonstrates an excitonic emission peak at ~514 nm with a full width at half-maximum (fwhm) of ~8 nm (Figure 2b). For the Yb-doped NPLs, a strong and broad emission in the NIR wavelength region (~724 nm, fwhm = 145 nm) was observed along with the narrow excitonic emission (~515 nm, fwhm = 9 nm).

In the inset image of Figure 2b, the PL intensity of undoped CdSe NPLs was multiplied 100 times. As seen in the PL spectrum, undoped 4 ML CdSe NPLs have a weak and broad trap-related emission, which peaks at ~675 nm. On the other hand, for Yb-doped 4 ML CdSe NPLs, the peak emission is at 724 nm. The difference in wavelength is nearly 50 nm between the trap-emission of CdSe NPLs and their dopant-related emission. Also, the slight red shift of the excitonic emission confirms that doped NPLs are slightly larger in the seeded growth at the second step of the reaction compared to undoped NPLs (also verified with TEM images). Here, NIR broad emission is attributed to Yb^{2+}-induced DE. Previously, broad-band emissions were observed for Cu- and Ag-doped CdSe NPLs, which were explained to be resulting from the recombination of delocalized electrons in the conduction band (CB) with strongly localized holes in dopant states.[19,36−38]

In order to understand the origins of different emission peaks in our doped NPLs, we conducted the PLE spectroscopy at different emission wavelengths (e.g., 515 nm for excitonic and 670 and 730 nm for broad DE) (Figure 2c). All three recorded PLE spectra have similar excitonic profiles, confirming that both excitonic and DE originated from the same 4 ML CdSe NPL hosts. Also, we measured the absolute PL QYs of all doped and undoped colloidal NPLs using an integrating sphere in hexane. Among the optical properties, the most dramatic change was observed in the QY between undoped and Yb-doped CdSe NPLs. While undoped NPLs had a QY of 28%, we observed a 96% increase in the overall PL QY, reaching 55% after doping. Moreover, for doped NPLs, we measured that the main contribution to improved QY originates from DE (~85%), while excitonic emission shows a decreased QY with respect to the undoped counterparts, which possibly indicates that the excitonic recombination is changed.

In order to understand the emission recombination mechanism for doped and undoped NPLs, time-resolved fluorescence (TRF) studies were conducted at excitonic and dopant-induced emissions. Figure S3 shows the TRF decay curves for undoped and Yb-doped NPLs at the excitonic emission peak. The average excitonic emission lifetime becomes faster after doping which indicates possible energy transfer to dopant ions. For the band-edge, there is a roughly 30% decrease (2.91 to 2.08 ns) in the averaged lifetime for doped NPLs compared to that of the undoped NPLs, which provides indirect insight into the change in the recombination process (Figure

https://doi.org/10.1021/acs.jpcc.2c09075
J. Phys. Chem. C 2023, 127, 4210−4217

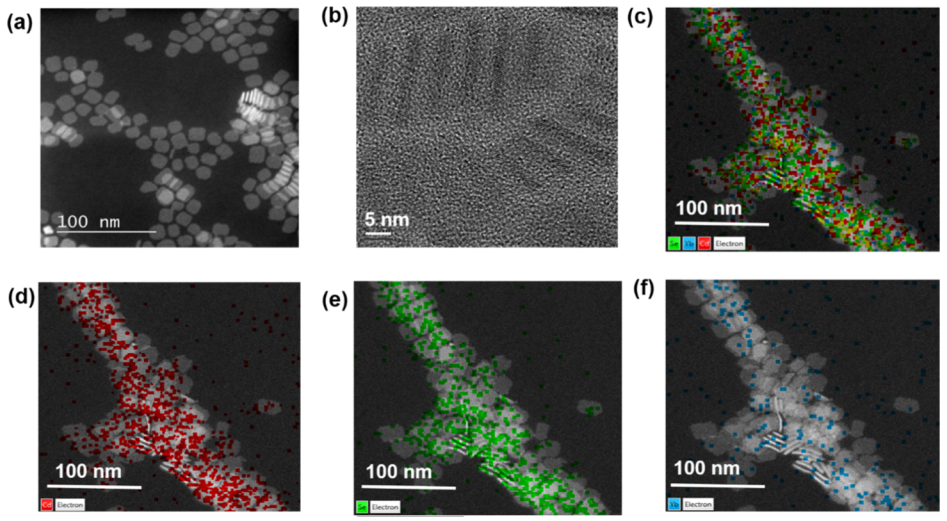

Figure 3. (a) HAADF−STEM image, (b) HR-TEM image, and EDX elemental mapping spectra of (c) combined and individually for (d) Cd, (e) Se, and (f) Yb elements from Yb-doped 4 ML CdSe core NPLs.

S3). Similar findings are reported in the literature for the PL lifetime for other doped NPLs.[18,20,21]

Furthermore, Figure 2d shows the comparison of TRF decay curves for efficient NIR emission for doped NPLs (~724 nm) with respect to weak intrinsic defects (~724 nm) for undoped NPLs. Yb-dopant-induced NIR emission exhibits an ~4 times longer amplitude-average PL lifetime (τ_{av} = 950 ns) in comparison to that for the undoped NPLs (τ_{av} = 260 ns). This tremendous increase in the average PL lifetime clearly indicates a change in the exciton recombination mechanism as compared to trap-related emission in undoped NPLs. Thus, Yb-dopant-induced emission is clearly different from the intrinsic defect emission of undoped 4 ML CdSe NPLs. However, the Yb^{2+} emission, generally appearing in the green region for inorganic phosphors, originates from the $4f^{13}5d^{1} \rightarrow 4f^{14}$ transition with an average lifetime between 100 and 1000 ns.[39−41] In our case, due to the lower bandgap of 4 ML CdSe NPLs as compared to that of inorganic phosphors, we could not observe any signs of this well-known $4f^{13}5d^{1} \rightarrow 4f^{14}$ transition of Yb^{2+} ions. Since there is no literature report on the doping of Yb ions in II−VI nanocrystals, we can speculate on the emission mechanism of Yb^{2+} ions in our 4 ML CdSe NPL hosts. There are two possibilities: (1) as in the previously reported dopant ions (e.g., Cu^{+}, Ag^{+}) in CdSe NPLs, the delocalized electron of the CB will recombine with any state of Yb-induced energy level resulting in efficient NIR emission and (2) Yb^{2+} dopant ions, by possessing larger ionic radii than that for Cd^{2+} ions in tetrahedral coordination, may result in increased lattice strain on the atomically flat 4 ML CdSe NPLs. This may give rise to strain-induced radiative mid-gap emission, which possesses a very long decay lifetime as compared to the inefficient intrinsic defect emission of undoped CdSe NPLs.

Additional elemental characterizations were performed to further confirm the presence of Yb^{2+} dopants in CdSe NPLs. The HAADF-STEM image of Yb-doped CdSe NPLs reveals a square shape with an average lateral size of 17.2 ± 1.3 nm, as seen in Figure 3a. For the undoped CdSe NPLs, we measured slightly smaller dimensions of 16.3 ± 1.5 nm, confirming seeded growth at the reaction's second step (Figure S4). Thicknesses of both undoped and Yb-doped NPLs were measured as ~1.3 nm from high-resolution TEM (HR-TEM) images in Figures 3b and S4. This confirms that the second step of the synthesis procedure leads to only lateral expansion rather than shell growth. Furthermore, the shape of NPLs remains the same after doping with Yb ions. The HAADF-STEM images with corresponding elemental mapping for Cd, Se, and Yb ions via EDX are shown in Figure 3c−f. As shown from the elemental mappings, Cd and Se are dispersed across the entire NPL structures, while Yb ions are only found at the sides rather than the centers of the NPLs, as expected from our seeded-growth method. Moreover, the chemical composition of Yb-doped core NPLs was also obtained from SEM−EDX analysis. Elemental percentages of Yb-doped CdSe NPLs (Yb-CdSe NPL-1) are Cd/Se/Yb—52.4:46.7:0.9 (Table S1). In the Yb^{2+} system, the electrons in the near-saturated 4f orbits of Yb^{2+} can jump into 6s or 5d orbits, which makes orbit groups (4f 6s and 4f 5d) couple and split, forming different energy levels, and thus the electrons can undergo this transition and decay by this change.[39] In our case, Yb^{2+} doping provides the PL signal of broad DE at 724 nm. The ionic radius of Yb^{2+} (0.116 nm)[40] is larger than that of Cd^{+2} (0.078 nm);[37] therefore, they form substitutional impurities and a Stokes-shifted-induced DE in colloidal nanocrystals. Additional XPS characterization is presented in Figure S5.

Finally, after the successful synthesis of the divalent Yb-doped 4 ML CdSe NPLs with an efficient NIR emission, additional experiments and characterization were undertaken to explore the DE mechanism systematically. As stated before, the second step of our reaction included the injection of Cd^{2+} and Se^{2-} ions also, so we needed to confirm that the NIR emission originated from Yb^{2+} dopants. Thus, as a control reaction, at the second step of the seeded-growth process, we used solely Cd^{2+} and Se^{2-} precursors (without the addition of Yb salt), keeping other reaction parameters the same. The absorption and PL spectra for the synthesized NPLs showed an ~2−3 nm red shift, indicating a slight lateral size growth as expected (Figure S6). The PL QY of this sample was ~10%. This control reaction confirmed that a broad NIR emission is impossible without Yb salt addition. As a second step to check the role of iodide, we designed another control reaction by replacing YbI_2 with the CdI_2 salt as a precursor for doping in CdSe NPLs.[30] Since both precursors contain iodide, the difference should come from the absence of Yb dopants compared to our original synthesis. Figure S7 shows absorption, PL spectra, and TEM images for the CdI_2-doped NPLs. The NPLs synthesized using the CdI_2 salt exhibit dual

https://doi.org/10.1021/acs.jpcc.2c09075
J. Phys. Chem. C 2023, 127, 4210−4217

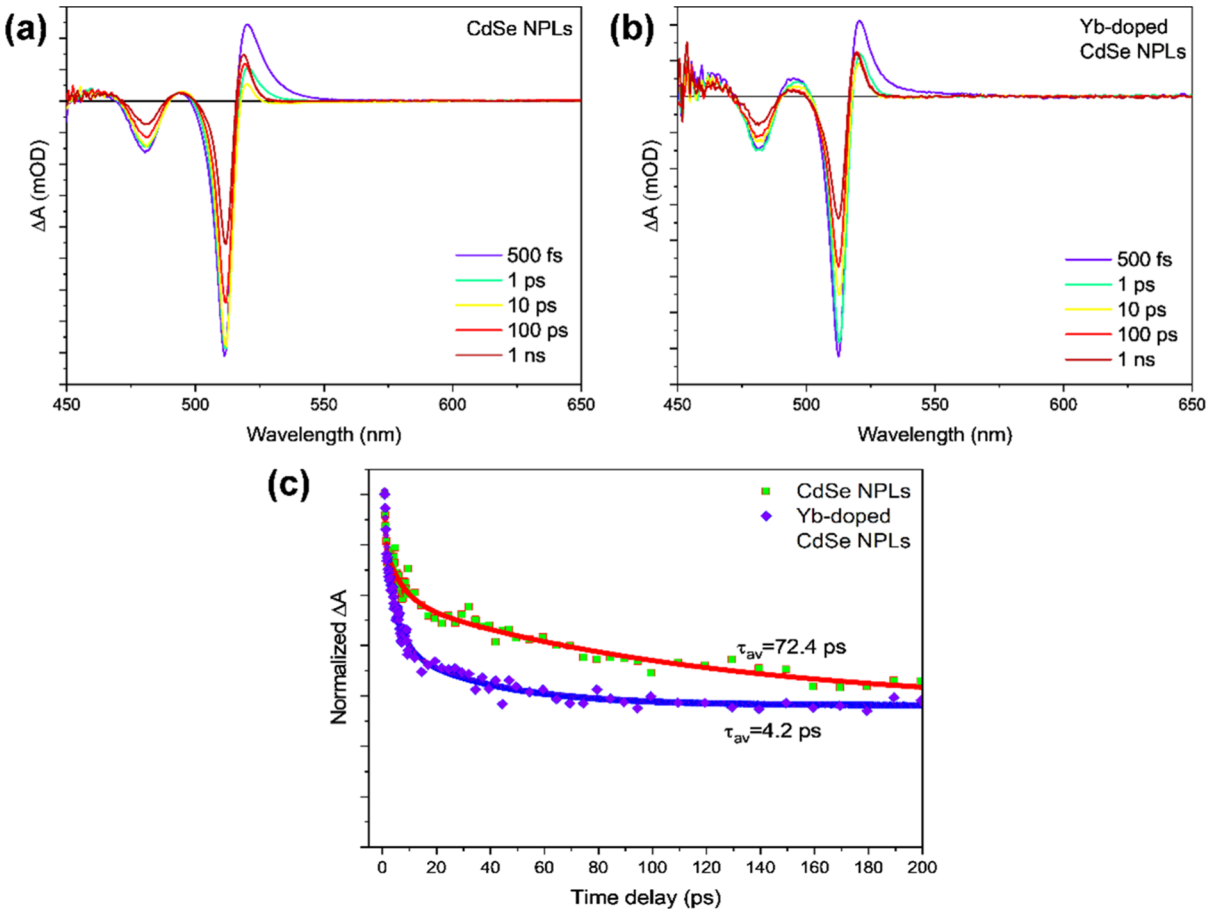

Figure 4. TA spectra at an increasing delay for (a) 4 ML CdSe NPLs and (b) Yb-doped 4 ML CdSe NPLs at 20 μJ/cm^2. (c) TA dynamics of 4 ML CdSe NPLs and 4 ML Yb-doped CdSe NPLs monitored at the heavy hole of CdSe NPLs (510 nm) at 20 μJ/cm^2.

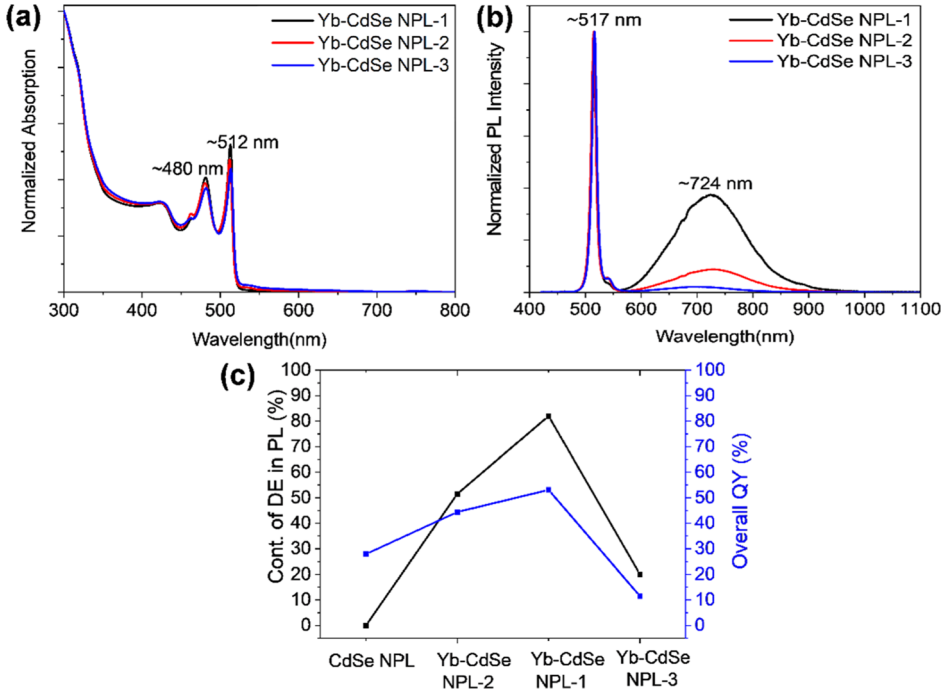

Figure 5. (a) Normalized absorption and (b) PL spectra of Yb-CdSe NPLs with a variable amount of YbI_2 dopants. (c) Contribution of DEs in PL and overall QY Yb-doped NPLs with increasing dopant amount.

https://doi.org/10.1021/acs.jpcc.2c09075
J. Phys. Chem. C 2023, 127, 4210−4217

emissions, one at ∼516 nm, which belongs to the excitonic emission of 4 ML CdSe NPLs, and the other at 540 nm. Additional Cd precursor may change the total Cd^{2+} to Se^{2-} ratio from our optimized 4 ML recipe. This can change the nucleation and growth process and result in a small extra growth of small 5 ML CdSe NPL populations as a by-product, which has a known emission of around 540 nm.[21] TEM images reveal that these NPLs have a similar size and shape compared to Yb-doped NPLs. However, their QY is around ∼10%, which is lower than that of undoped CdSe NPLs (QY ∼ 28%). The amplitude-average fluorescence lifetime obtained from TRF spectroscopy was ∼4.35 ns at 515 nm (see Figure S8 and Table S2). Thus, our control experiments provide a strong supporting evidence that the QY enhancement of Yb-doped NPLs is related to the Yb-doping process, which creates an additional radiative recombination channel in the NIR region apart from the excitonic emission peak.

To understand dopant-related changes, we further investigated the doped and undoped NPLs using TA spectroscopy. For 4 ML CdSe NPLs, the depopulation of the electrons in the CB is mainly determined by electron trapping and radiative/nonradiative recombination of excitons.[41] We monitored the TA dynamics of these undoped and Yb-doped 4 ML CdSe NPLs at the heavy hole of CdSe NPLs (512 nm) (Figure 4a,b). We used a triexponential decay to fit the TA curve and calculate the recovery of the bleaching of undoped and Yb-doped NPLs (Figure 4c). In Yb-doped NPLs, the bleach recovery had an additional contribution from exciton−Yb energy transfer. The Yb-doped NPLs exhibited a faster recovery of bleaching with 4.2 ps compared to undoped NPLs with 72.4 ps. The fast recovery of the bleaching confirms the exciton-Yb energy transfer process, which is much faster than the other radiative and nonradiative relaxation pathways. The combination of a faster decay in the TA spectra and a slower PL lifetime was also previously reported in the literature and attributed to doped nanoparticles.[41−43]

Different doping concentrations were further investigated experimentally to examine the influence of the Yb^{2+} dopant concentration on DE. Figure 5a,b shows normalized absorption and PL spectra of Yb-doped CdSe NPLs, synthesized with the increasing amount of YbI_2 with the labels: Yb-doped CdSe NPL-1, -2, and -3. For the studied doping concentrations, we did not observe any significant variation in the steady-state absorption profiles (Figure 5a). Steady-state PL emission spectra reveal that excitonic emission remains the same for the different doped samples. However, for DE, we observed a very slight blue shift with increasing dopant amounts (Figures 5b and S9), which was more evident when we normalized the spectra at the DE peak. The most dramatic difference between the samples was observed in the intensity of DE and its contribution over QY with the change in the doping amount, as seen in Figure 5c.

QY is an important indicator of the emissive properties, which quantifies the ratio of the emitted to the absorbed photons. The most dramatic difference between the samples was observed with the intensity of DE and its contribution to QY with the change in the doping amount, as seen in Figure 5c. QY comparison of Yb-doped samples and comparison of the DE contribution clearly show that the Yb-doping process influences the exciton recombination process. In the case of doped NPLs, we also find the individual contributions of radiative channels (excitonic and DE). For undoped CdSe NPLs, the QY was measured as ∼28%, where the radiative channel is only the excitonic emission at 514 nm. In the case of Yb-doped NPLs, we observed that DE was the main contributor to the total radiative emission, which was also reported previously for Cu- and Ag-doped NPLs.[13,16,19−21] The highest QY of 55% was achieved for the sample named Yb-CdSe NPL-1 synthesized by using 0.16 mmol of YbI_2 (Figure 5c). The Yb-CdSe NPL-2 and Yb-CdSe NPL-3 samples synthesized using 0.08 and 0.32 mmol YbI_2 possessed PL QYs of ∼45 and 20%, respectively. Further, Figure 5c shows the DE contribution to the total emission, which is calculated by integrating the emission contribution of DE with respect to the overall emission (i.e., dopant + excitonic). Thus, the change in QY for different samples is correlated with the contribution of DE to the overall emission spectrum. The decay curves for the Yb-CdSe NPL-2 and Yb-CdSe NPL-3 samples show microsecond-long decay curves with an average lifetime of 330−1220 ns (Figures S10 and S11 and Tables S3 and S4).

CONCLUSIONS

In conclusion, divalent Yb-doped 4 ML CdSe NPLs have been synthesized via a seeded-growth method for the first time. Doped NPLs were optimized to show enhanced DE by changing the doping concentrations. The overall PL QY of the doped NPLs possessing emission in the visible to the NIR regions was doubled as compared to that of the undoped NPLs. We have carried out detailed elemental and optical characterizations to confirm successful doping and its emerging optoelectronic properties. The presented method for Yb-doping in CdSe NPLs can be employed for other divalent lanthanides to expand the library of unexplored lanthanide-doped II-VI nanocrystals.

ASSOCIATED CONTENT

Supporting Information

The Supporting Information is available free of charge at https://pubs.acs.org/doi/10.1021/acs.jpcc.2c09075.

Additional UV, PL, TRF, XPS, SEM−EDX, and TA measurements and HAADF−TEM images for Yb-doped CdSe NPLs (PDF)

AUTHOR INFORMATION

Corresponding Author

Hilmi Volkan Demir − *LUMINOUS! Centre of Excellence for Semiconductor Lighting and Displays, the Photonics Institute, School of Electrical and Electronic Engineering, School of Physical and Mathematical Sciences, School of Materials Science and Engineering, Nanyang Technological University, Singapore 639798, Singapore; Department of Electrical and Electronics Engineering, Department of Physics, UNAM—Institute of Materials Science and Nanotechnology and National Nanotechnology Research Center, Bilkent University, Ankara 06800, Turkey;* orcid.org/0000-0003-1793-112X; Email: hvdemir@ntu.edu.sg

Authors

Merve İzmir − *LUMINOUS! Centre of Excellence for Semiconductor Lighting and Displays, the Photonics Institute, School of Electrical and Electronic Engineering, School of Physical and Mathematical Sciences, School of Materials Science and Engineering, Nanyang Technological University, Singapore 639798, Singapore;* orcid.org/0000-0001-8602-0106

Emek G. Durmusoglu − *LUMINOUS! Centre of Excellence for Semiconductor Lighting and Displays, the Photonics Institute, School of Electrical and Electronic Engineering, School of Physical and Mathematical Sciences, School of Materials*

https://doi.org/10.1021/acs.jpcc.2c09075
J. Phys. Chem. C 2023, 127, 4210−4217

Science and Engineering, Nanyang Technological University, Singapore 639798, Singapore; orcid.org/0000-0001-6840-8342

Manoj Sharma − *LUMINOUS! Centre of Excellence for Semiconductor Lighting and Displays, the Photonics Institute, School of Electrical and Electronic Engineering, School of Physical and Mathematical Sciences, School of Materials Science and Engineering, Nanyang Technological University, Singapore 639798, Singapore; ARC Centre of Excellence in Exciton Science, Department of Materials Science and Engineering, Monash University, Melbourne, Victoria 3800, Australia;* orcid.org/0000-0001-5215-9740

Farzan Shabani − *Department of Electrical and Electronics Engineering, Department of Physics, UNAM—Institute of Materials Science and Nanotechnology and National Nanotechnology Research Center, Bilkent University, Ankara 06800, Turkey;* orcid.org/0000-0003-2174-5960

Furkan Isik − *Department of Electrical and Electronics Engineering, Department of Physics, UNAM—Institute of Materials Science and Nanotechnology and National Nanotechnology Research Center, Bilkent University, Ankara 06800, Turkey;* orcid.org/0000-0001-5881-5438

Savas Delikanli − *Department of Electrical and Electronics Engineering, Department of Physics, UNAM—Institute of Materials Science and Nanotechnology and National Nanotechnology Research Center, Bilkent University, Ankara 06800, Turkey;* orcid.org/0000-0002-0613-8014

Vijay Kumar Sharma − *LUMINOUS! Centre of Excellence for Semiconductor Lighting and Displays, the Photonics Institute, School of Electrical and Electronic Engineering, School of Physical and Mathematical Sciences, School of Materials Science and Engineering, Nanyang Technological University, Singapore 639798, Singapore; Department of Electrical and Electronics Engineering, Department of Physics, UNAM—Institute of Materials Science and Nanotechnology and National Nanotechnology Research Center, Bilkent University, Ankara 06800, Turkey;* orcid.org/0000-0002-2028-5715

Complete contact information is available at: https://pubs.acs.org/10.1021/acs.jpcc.2c09075

Author Contributions

M.I. and E.G.D. contributed equally. The article was written with the contributions of all authors. All authors have approved the final version of the article.

Notes

The authors declare no competing financial interest.

■ ACKNOWLEDGMENTS

This research was supported by the Ministry of Education, Singapore, under its Academic Research Fund Tier 1 (MOE-RG62/20), Singapore Agency for Science, Technology and Research (A*STAR) MTC program, grant no. M21J9b0085, and partly from TUBITAK 119N343, 120N076, 121N395, and 20AG001. H.V.D. also acknowledges the support from TUBA. We also thank Dr Sushant Shendre (Nanyang Technological University) for his early assistance with the synthesis work and Hamed Dehghanpour Baruj (Bilkent University) for his assistance with the XPS measurement.

■ REFERENCES

(1) Sharma, M. K.; Delikanli, S.; Demir, H. V. Two-Dimensional CdSe-Based Nanoplatelets: Their Heterostructures, Doping, Photophysical Properties, and Applications. *Proc.—IEEE* **2020**, *108*, 655−675.

(2) Kelestemur, Y.; Shynkarenko, Y.; Anni, M.; Yakunin, S.; De Giorgi, M. L.; Kovalenko, M. V. Colloidal CdSe Quantum Wells with Graded Shell Composition for Low-Threshold Amplified Spontaneous Emission and Highly Efficient Electroluminescence. *ACS Nano* **2019**, *13*, 13899−13909.

(3) Luo, S.; Kazes, M.; Lin, H.; Oron, D. Strain-Induced Type-II Band Alignment Control in CdSe Nanoplatelet/ZnS-Sensitized Solar Cells. *J. Phys. Chem. C* **2017**, *121*, 11136−11143.

(4) Sharma, M.; Gungor, K.; Yeltik, A.; Olutas, M.; Guzelturk, B.; Kelestemur, Y.; Erdem, T.; Delikanli, S.; McBride, J. R.; Demir, H. V. Near-Unity Emitting Copper-Doped Colloidal Semiconductor Quantum Wells for Luminescent Solar Concentrators. *Adv. Mater.* **2017**, *29*, 1700821.

(5) Guzelturk, B.; Kelestemur, Y.; Olutas, M.; Delikanli, S.; Demir, H. V. Amplified Spontaneous Emission and Lasing in Colloidal Nanoplatelets. *ACS Nano* **2014**, *8*, 6599−6605.

(6) Liu, B.; Sharma, M.; Yu, J.; Shendre, S.; Hettiarachchi, C.; Sharma, A.; Yeltik, A.; Wang, L.; Sun, H.; Dang, C.; et al. Light-Emitting Diodes with Cu-Doped Colloidal Quantum Wells: From Ultrapure Green, Tunable Dual-Emission to White Light. *Small* **2019**, *15*, 1901983.

(7) Lhuillier, E.; Dayen, J.-F.; Thomas, D. O.; Robin, A.; Ithurria, S.; Aubin, H.; Dubertret, B. Phototransport in Colloidal Nanoplatelets Array. *Phys. Status Solidi C* **2016**, *13*, 526−529.

(8) Lee, J.; Yoo, K.; Liu, H.; Kang, J. Use of 2D Nanoplatelets to Improve The Sensitivity in Hybrid Photodetector for Indirect X-Ray Imaging. *Res. Sq.* **2021**, *1*, 1−18.

(9) Ithurria, S.; Tessier, M. D.; Mahler, B.; Lobo, R. P.; Dubertret, B.; Efros, A. L. Colloidal Nanoplatelets with Two-dimensional Electronic Structure. *Nat. Mater.* **2011**, *10*, 936−941.

(10) Izmir, M.; Sharma, A.; Shendre, S.; Durmusoglu, E. G.; Sharma, V. K.; Shabani, F.; Baruj, H. D.; Delikanli, S.; Sharma, M.; Demir, H. V. Blue-Emitting CdSe Nanoplatelets Enabled by Sulfur-Alloyed Heterostructures for Light-Emitting Diodes with Low Turn-on Voltage. *ACS Appl. Nano Mater.* **2022**, *5*, 1367−1376.

(11) Altintas, Y.; Quliyeva, U.; Gungor, K.; Erdem, O.; Kelestemur, Y.; Mutlugun, E.; Kovalenko, M. V.; Demir, H. V. Highly Stable, Near-Unity Efficiency Atomically Flat Semiconductor Nanocrystals of CdSe/ZnS Hetero-Nanoplatelets Enabled by ZnS-Shell Hot-Injection Growth. *Small* **2019**, *15*, 1804854.

(12) Meerbach, C.; Tietze, R.; Voigt, S.; Sayevich, V.; Dzhagan, V. M.; Erwin, S. C.; Dang, Z.; Selyshchev, O.; Schneider, K.; Zahn, D. R. T.; et al. Brightly Luminescent Core/Shell Nanoplatelets with Continuously Tunable Optical Properties. *Adv. Opt. Mater.* **2019**, *7*, 1801478.

(13) Sharma, M.; Olutas, M.; Yeltik, A.; Kelestemur, Y.; Sharma, A.; Delikanli, S.; Guzelturk, B.; Gungor, K.; McBride, J. R.; Demir, H. V. Understanding the Journey of Dopant Copper Ions in Atomically Flat Colloidal Nanocrystals of CdSe Nanoplatelets Using Partial Cation Exchange Reactions. *Chem. Mater.* **2018**, *30*, 3265−3275.

(14) Antanovich, A.; Yang, L.; Erwin, S. C.; Martín-García, B.; Hübner, R.; Steinbach, C.; Schwarz, D.; Gaponik, N.; Lesnyak, V. $CdSe_xS_{1-x}$ Alloyed Nanoplatelets with Continuously Tunable Blue-Green Emission. *Chem. Mater.* **2022**, *34*, 10361−10372.

(15) Schimpf, A. M.; Knowles, K. E.; Carroll, G. M.; Gamelin, D. R. Electronic Doping and Redox-potential Tuning in Colloidal Semiconductor Nanocrystals. *Acc. Chem. Res.* **2015**, *48*, 1929−1937.

(16) Bedil, M. S.; Vladimir, B. Z.; Mikhail, V. B.; Roman, B. V. Highly Luminescent Copper-doped Ultrathin CdSe Nanoplatelets for White-light Generation. *J. Lumin.* **2020**, *222*, 117134.

(17) Knowles, K. E.; Hartstein, K. H.; Kilburn, T. B.; Marchioro, A.; Nelson, H. D.; Whitham, P. J.; Gamelin, D. R. Luminescent Colloidal Semiconductor Nanocrystals Containing Copper: Synthesis, Photophysics, and Applications. *Chem. Rev.* **2016**, *116*, 10820−10851.

(18) Whitham, P. J.; Knowles, K. E.; Reid, P. J.; Gamelin, D. R. Photoluminescence Blinking and Reversible Electron Trapping in Copper-Doped CdSe Nanocrystals. *Nano Lett.* **2015**, *15*, 4045−4051.

(19) Najafi, A.; Sharma, M.; Delikanli, S.; Bhattacharya, A.; Murphy, J. R.; Pientka, J.; Sharma, A.; Quinn, A. P.; Erdem, O.; Kattel, S.;

Kelestemur, Y.; Kovalenko, M. V.; et al. Light-Induced Paramagnetism in Colloidal Ag^{+}-Doped CdSe Nanoplatelets. *J. Phys. Chem. Lett.* **2021**, *12*, 2892−2899.
(20) Dufour, M.; Izquierdo, E.; Livache, C.; Martinez, B.; Silly, M. G.; Pons, T.; Lhuillier, E.; Delerue, C.; Ithurria, S. Doping as a Strategy to Tune Color of 2D Colloidal Nanoplatelets. *ACS Appl. Mater. Interfaces* **2019**, *11*, 10128−10134.
(21) Sharma, A.; Sharma, M.; Gungor, K.; Olutas, M.; Dede, D.; Demir, H. V. Near-Infrared-Emitting Five-Monolayer Thick Copper-Doped CdSe Nanoplatelets. *Adv. Opt. Mater.* **2019**, *7*, 1900831.
(22) Khan, A. H.; Pinchetti, V.; Tanghe, I.; Dang, Z.; Martín-García, B.; Hens, Z.; van Thourhout, D.; Geiregat, P.; Brovelli, S.; Moreels, I. Tunable and Efficient Red to Near-Infrared Photoluminescence by Synergistic Exploitation of Core and Surface Silver Doping of CdSe Nanoplatelets. *Chem. Mater.* **2019**, *31*, 1450.
(23) Guozhu, S.; Baojiu, C.; Xizhen, Z.; Xiangping, L.; Jinsu, Z.; Sai, X.; Jiashi, S.; Yongze, C.; Xin, W.; Yanqiu, Z.; Yuhang, Z.; Xiangqing, Z. Radiative Transition Properties of Yb^{3+} in Er^{3+}/Yb^{3+} Co-doped $NaYF_4$ Phosphor. *J. Alloys Compd.* **2020**, *834*, 155242.
(24) Mir, W. J.; Sheikh, T.; Arfin, H.; Xia, Z.; Nag, A. Lanthanide Doping in Metal Halide Perovskite Nanocrystals: Spectral Shifting, Quantum Cutting and Optoelectronic Applications. *NPG Asia Mater.* **2020**, *12*, 9.
(25) Martín-Rodríguez, R.; Geitenbeek, R. G.; Meijerink, A. Incorporation and Luminescence of Yb^{3+} in CdSe Nanocrystals. *J. Am. Chem. Soc.* **2013**, *135*, 13668−13671.
(26) Rutstrom, D.; Stand, L.; Dryzhakov, B.; Koschan, M.; Melcher, C. L.; Zhuravleva, M. Crystal Growth and Scintillation Properties of New Ytterbium-activated Scintillators Cs_4CaI_6: Yb and Cs_4SrI_6: Yb. *Opt. Mater.* **2020**, *110*, 110536.
(27) Suta, M.; Wickleder, C. Spin Crossover of Yb^{2+} in $CsCaX_3$ and $CsSrX_3$ (X = Cl, Br, I) − A Guideline to Novel Halide-Based Scintillators. *Adv. Funct. Mater.* **2017**, *27*, 1602783.
(28) Katyayan, S.; Agrawal, S. Optical Behaviour of Eu^{2+} and Yb^{2+} Doped Alkaline Earth Metatitanate Perovskite Phosphors. *Optik* **2020**, *219*, 165284.
(29) Tessier, M. D.; Javaux, C.; Maksimovic, I.; Loriette, V.; Dubertret, B. Spectroscopy of Single CdSe Nanoplatelets. *ACS Nano* **2012**, *6*, 6751−6758.
(30) Galle, T.; Kazes, M.; Hübner, R.; Lox, J. F.; Samadi Khoshkhoo, M.; Sonntag, L.; Tietze, R.; Sayevich, V.; Oron, D.; Koitzsch, A.; Lesnyak, V.; et al. Colloidal Mercury-Doped CdSe Nanoplatelets with Dual Fluorescence. *Chem. Mater.* **2019**, *31*, 5065−5074.
(31) Zhou, D.; Liu, D.; Pan, G.; Chen, X.; Li, D.; Xu, W.; Bai, X.; Song, H. Cerium and Ytterbium Codoped Halide Perovskite Quantum Dots: A Novel and Efficient Downconverter for Improving the Performance of Silicon Solar Cells. *Adv. Mater.* **2017**, *29*, 1704149.
(32) Milstein, T. J.; Kroupa, D. M.; Gamelin, D. R. Picosecond Quantum Cutting Generates Photoluminescence Quantum Yields over 100% in Ytterbium-Doped $CsPbCl_3$ Nanocrystals. *Nano Lett.* **2018**, *18*, 3792−3799.
(33) Dorenbos, P. f → d Transition Energies of Divalent Lanthanides in Inorganic Compounds. *J. Phys.: Condens. Matter* **2003**, *15*, 575−594.
(34) Yeltik, A.; Olutas, M.; Sharma, M. K.; Gungor, K.; Demir, H. V. Nonradiative Energy Transfer between Doped and Undoped Flat Semiconductor Nanocrystals of Colloidal Quasi-2D Nanoplatelets. *J. Phys. Chem. Lett. C* **2019**, *123*, 1470−1476.
(35) Ithurria, S.; Tessier, M.; Mahler, B.; Lobo, R. P. S. M.; Dubertret, B.; Efros, A. L. Colloidal Nanoplatelets with Two-Dimensional Electronic Structure. *Nat. Mater.* **2011**, *10*, 936−941.
(36) Yu, J.; Sharma, M.; Wang, Y.; Delikanli, S.; Baruj, H. D.; Sharma, A.; Demir, H. V.; Dang, C. Modulating Emission Properties in a Host−Guest Colloidal Quantum Well Superlattice. *Adv. Opt. Mater.* **2022**, *10*, 2101756.
(37) Khan, A. H.; Pinchetti, V.; Tanghe, I.; Dang, Z.; Martín-García, B.; Hens, Z.; van Thourhout, D.; Geiregat, P.; Brovelli, S.; Moreels, I. Tunable and Efficient Red to Near-Infrared Photoluminescence by Synergistic Exploitation of Core and Surface Silver Doping of CdSe Nanoplatelets. *Chem. Mater.* **2019**, *31*, 1450.
(38) Hughes, K. E.; Hartstein, H. H.; Gamelin, D. R. Photodoping and Transient Spectroscopies of Copper-Doped CdSe/CdS Nanocrystals. *ACS Nano* **2018**, *12*, 718−728.
(39) Tomala, R.; Grzeszkiewicz, K.; Hreniak, D.; Strek, W. Downconversion process in Yb^{3+}doped GdAG nanocrystals. *J. Lumin.* **2018**, *193*, 70−72.
(40) Solomonov, V.; Osipov, V.; Spirina, A. Luminescence of Yb-doped YAG: Divalent ytterbium ions. *J. Lumin.* **2016**, *169*, 151−155.
(41) Chen, H. Y.; Maiti, S.; Son, D. H. Doping Location-dependent Energy Transfer Dynamics in Mn-doped CdS/ZnS Nanocrystals. *ACS Nano* **2012**, *6*, 583−591.
(42) Wang, Y.; Wu, B.; Yang, C.; Liu, M.; Sum, T. C.; Yong, K. T. Synthesis and Characterization of Mn:ZnSe/ZnS/ZnMnS Sandwiched QDs for Multimodal Imaging and Theranostic Applications. *Small* **2016**, *12*, 534−546.
(43) Xu, R.; Liao, C.; Xu, Y.; Zhang, C.; Xiao, M.; Zhang, L.; Lu, C.; Cui, Y.; Zhang, J. Bright Type-II Photoluminescence from Mn-doped CdS/ZnSe/ZnS Quantum Dots with $Mn^{(2+)}$ Ions as Exciton Couplers. *Nanoscale* **2017**, *9*, 18281−18289.

https://doi.org/10.1021/acs.jpcc.2c09075
J. Phys. Chem. C 2023, 127, 4210−4217